Studying Alpha Irradiated CR39 Using Positron Annihilation Spectroscopy

S. Limam[a,*], A. Guittoum[b], Z. Lounis-Mokrani[b], M. Hemous[b] and N. Bendjedda[2]

[a] *UR-MPE, M'hamed Bougara University, Boumerdes 35000, Algeria*
[b] *Nuclear Research Centre of Algiers, 02 Bd Frantz Fanon, BP 399, Alger-Gare, Algiers, Algeria*

Received: 08.05.2023 & Accepted: 21.08.2023

Doi: 10.12693/APhysPolA.144.163 *e-mail: s.limam@univ-boumerdes.dz

The monitoring of the alpha irradiation effect on the microstructural deformation of CR39 via the variation of free volumes has been studied. CR39 samples have been irradiated with alpha particles at fluencies Φ of 2.6×10^8, 5.27×10^8, 7.91×10^8, 1.3×10^9, 1.84×10^9, and 3.6×10^9 α/cm^2. The samples have been investigated with positron annihilation lifetime spectroscopy and Doppler broadening spectroscopy. The analysis of positron annihilation spectra has shown a variation of the ortho-positronium component τ_3 and the parameters S and W as a function of the fluence Φ. This variation is related to a change in the size and number of free volumes, which is created via the evolution of chemical chains. From the values of τ_3, the free volume radius has been estimated using the Tao–Eldrup model. Moreover, theoretical calculation of the radial dose distribution has been also performed using the Waligorski formulation to get the track core radius. After an etching of 5 min, the positron annihilation spectroscopy technique was again used to investigate the microstructural changes in etched samples subjected to alpha radiation. A clear variation of τ_3, S and W parameters, and free volume radius has been noted when compared to the non-etched samples.

topics: alpha particles, free volume radius, o-Ps lifetime, S-parameter

1. Introduction

Polyallyldiglycol carbonate ($C_{12}H_{18}O_7$), or CR39, is an amorphous polymer. It is a particular type of solid-state nuclear track detector (SSNTD), distinguished by its capacity to record charged particles as alpha in the form of latent tracks [1, 2]. The heavy charged particles interact with the chains of CR39 via ionization and/or excitation of electrons. This interaction occurs within a time order of 10^{-18} s [3, 4]. Thereafter, a new chemical species might be formed attending the stabilization, where a variety of events such as cross-linking, chain scission, or radical generation may take place [5], leading to the formation of nuclear tracks along the particle trajectories.

The simulation of alpha-induced damages in CR39 with the SRIM program [6] gives us the range where the energy will be disposed, which is around 30 μm for $E_\alpha = 5$ MeV. In addition, it is possible to calculate linear energy transfer (LET), used for predicting the structural deformation [5, 7]. However, using the SRIM program solely is not enough to simulate the damage distribution, because one considers only the linear transformation, i.e., the thing that does not express the ultimate structural modification. On a different note, the delta rays theory provides an accurate dose distribution around the particle's path, thanks to which the prediction of the track core radii could be realized [8–10]. Indeed, the energy loss due to primary electrons will be around the particle's path for only a few angstroms. In contrast, the secondary electrons transfer the energy up to a few microns away from the particle's path. Therefore, Katz and Kobetich [11] have established a model based on the delta function that restricts the included number of hits. The hit is the quantum that reflects the effect of the radiation [12]. The approach mimics the local dose distribution as a function of radial distance, enabling the simulation of the track core radii where the radiation damage dose reaches its highest value. Lounis-Mokrani et al. [13] show how the SANS technique has been used to validate this method experimentally. Latent tracks, birth tracks, and revealed tracks are the three distinct kinds of nuclear tracks. Latent tracks, which have diameters of the order of angstroms, are produced directly by irradiation on untreated CR39. After a brief period of etching, birth tracks become visible and can be seen as tracks that have diameters of only a few micrometers. After extensive etching, revealed tracks develop [14, 15]. Hence, the tracks' dimensions determine the monitoring technique. For example, the small angle neutron scattering (SANS) and small angle X-ray scattering (SAXS) techniques

provide the radial damage distribution of the latent tracks [13, 16, 17]. The chemical structure can be studied using the ultraviolet-visible (UV) technique, where the cross-linking can be quantified [4, 13, 18]. The quantification of radicals formation and scission of bonds can be analyzed by means of infrared (IR) and electron spin resonance (ESR) [4, 13, 19, 20]. The monitoring of the tracks can also be performed via the monitoring of the etched tracks, which uses chemical etching, where the tracks are studied by analyzing the variation of the different track-etch parameters (length, diameter, track density, track etch rate,...) obtained from the optical microscopy (OM) against the time of etching and/or the properties of the penetrating particles as done in the following works [21–24]. For example, in [13], the authors use 5 to 25 min of etching towards the visualization of the birth tracks using the scanning electron microscope (SEM).

Once the positron annihilation spectroscopy (PAS) technique has been recognized as a nuclear probe technique [25], it was found that the monitoring of the latent tracks can be achieved by pursuing the evolution of free volumes [26]. The free volumes in polymers are generated on redistribution upon molecular chain packing [27, 28]; such an effect can be the result of radiation damage. Knowing that the free volumes could exist in time ranging between 10^{-13} and 10^{-16} s with a dimension of 1–10 Å, PAS seems to be a unique tool to probe the growth of free volumes [29, 30]. In the positron annihilation lifetime spectroscopy (PALS) method, when a positron interacts with matter, it could be backscattered from the surface or lose its energy through a different process of slowing down for thermalization. The thermalized positrons get diffused in the medium, where an annihilation with electrons might occur in bulk or inside the defects [31]. According to the Doppler effect, emitted photons could therefore slightly change their direction and broaden to the opposite 180° angle. When a positron and an electron are in close contact in areas with low electron densities, they can create the unstable bound state positronium (Ps). The creation of Ps happens mostly in porous materials like zeolites or metal-organic frameworks and at local free volumes between molecules [32, 33]. The positronium has a size of $1.59A^{\circ}$ and is characterized by a lifetime on a nano-second scale. So, the non-static appearance of molecular motion may be tracked in an unprecedented way [32]. The ground state of Ps consists of two distinct spin arrangements. Spin zero describes the singlet state or parapositronium (p-Ps). It is created when the spins of the positron and electron line up in opposition to one another, producing a total spin of zero. On the other hand, the ortho-positronium (o-Ps) state is three triplet spin state with a total spin of one [34]. The creation of Ps is made essentially by the dynamics of electron–radical recombination, the affinity of host material for electrons, and the ability of the environment to block electron–positron attraction. There exist a number of models concerning the formation of positronium, for example, the blob model and the spur model. The model adopted in our case study is the so-called Ore gap model. The latter is dependent on the ionization energy of the medium (I) and the binding energy of Ps (E_{Ps}). The positron kinetic energy E must belong to interval $I > E > I - E_{\mathrm{Ps}}$ [35] to exist. The best theoretical value for o-Ps lifetime in vacuum is 142.08 ns, and its best experimentally found value is 141.88 ns [36]. The most important detectable annihilated gamma comes from the pick-off process. The pick-off process is the annihilation of the positron forming the o-Ps by an electron from the host material via two photons of gamma. Depending on the local electron density and size of the open volume defects, the o-Ps lifetime typically varies during that operation from 1–10 ns [37]. In the literature, Dlubek et al. [27, 32, 38, 39], Lounis-Mokrani et al. [40], and Kumar et al. [5, 41–43] did several investigations concerning the characterization of irradiation-induced free volume growth in CR39 and other polymers using the correlation of o-Ps lifetime with free volume dimensions, and they got an interesting interpretation that allows the CR39 scientific community to understand better the nature of radiations damages.

In our case, we intend to monitor the latent tracks induced by alpha particles on CR39 by studying the variation of the properties of the free volumes using the correlation of o-Ps lifetime with their dimensions and pursuing the electron-positron momentum distribution by S/W-parameter. Then, the analysis is repeated after 5 min of an etching operation. A radial dose distribution calculation using the Waligorski formula has been done to confirm the experimental results.

2. Experimental procedure

2.1. Irradiation

The CR-39 used is manufactured by Pershore Mouldings Ltd. (UK) and has a thickness of 500 μm. The irradiations have been performed using ^{239}Pu as a radioactive source of alpha particles (5.1 MeV) with a collimator of 1 cm, yielding an energy of 4.1 MeV. For practical purposes, six pairs of CR39 have been irradiated for 1, 2, 3, 5, 7, and 14 days to obtain the following fluencies: 2.6×10^8, 5.27×10^8, 7.91×10^8, 1.3×10^9, 1.84×10^9, and 3.6×10^9 α/cm^2.

2.2. Positron annihilation spectroscopy measurements

The PAS measurements were carried out at the Nuclear Research Centre of Algiers (CRNA) using two spectrometers. The first was the PALS

system, which uses a conventional fast–fast coincidence system made by a detecting system composed of two identical cylindrical plastic scintillators BC418 manufactured by BICRON coupled to Burle 8850 photomultiplier tubes (PMT) purchased from ORTEC. The sandwich geometry was assumed there; two stacked layers of the samples were put on both sides of the positron-emitting radioactive ^{22}Na source with activity of 20 μCi deposited on a Kapton sheet of a thickness of 25 μm [44].

The positron lifetime spectra were acquired by collecting 2×10^6 annihilation events with a time resolution of 0.270 ± 0.00049 ns. The second spectrometer is the DBS, where the detection of Doppler broadening spectrums of 511 keV photon gamma annihilation was carried out with HP-Ge (high-purity germanium) coaxial detector system having the resolution of 1.6 keV for 1.33 MeV, ^{60}Co.

An operation of chemical etching was conducted using a KOH (potassium hydroxide) solution for a duration of 5 min. The samples were immersed in a thermal bath containing a basic solution to carry out chemical etching. The solution was continuously agitated during the etching procedure to guarantee their homogeneity. The concentration and temperature values were optimized to be $C = 6.25$ N and $T = 70 \pm 2$°C according to [45, 46]. The etching rate accelerates exponentially as the temperature and concentration rise. This behavior demonstrates the sensitivity of the etching process to temperature and concentration variations, which can greatly affect how quickly material is removed [24, 47]. After the etching process, the detectors were properly cleaned in distilled water and dried to stop the etching process and remove the components of the basic solution. The PALS and DBS measurements have been performed in the same conditions for the etched samples.

3. Results and discussion

3.1. Doppler broadening spectra (DBS) analysis

Using Doppler broadening spectra, the longitudinal momentum density component can be characterized qualitatively via the measure of the full width at half maximum (FWHM) of the photon gamma for the annihilated positrons of 511 keV [37]. Since the positrons are already thermalized, this will reflect the electron density momentum distribution at the annihilation sites. The characterization is well established via the parameters of shape (S — shape parameter) and wings (W — wing parameter), which are demonstrated in Fig. 1.

In fact, S is expressed as the ratio of the centered integrated area, dS, to the full integrated area of the 511 keV energetic spectrum, dA. The parameter W, on the other hand, is the ratio of counts in the off-center fraction, dW, divided by the entire area of the annihilation spectrum [48, 49]. The fit of the

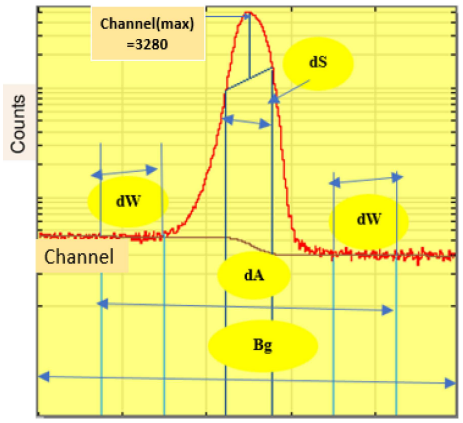

Fig. 1. Parameters S and W.

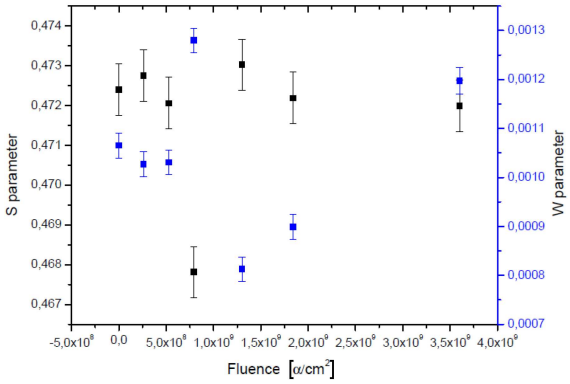

Fig. 2. Variation of parameters S and W vs fluence.

DBS spectra is well done using the SP program from J. Dryzek [50, 51]. The parameters S and W were calculated with an error of 10^{-4}.

The SP program has an easy implementation and automatically calculates S and W parameters by deducting the background. The based algorithm can fit a Gaussian curve to the spectrum, and the position for the maximum of the Gaussian curve matches the 511 keV position. Therefore, the integration ranges for the parameters S and W are determined. The S-parameter with values up to 0.5 is sensitive to the annihilation with low momentum valence and unbound electrons — hence the increase in the value of S-parameter indicates the annihilation of positrons with those electrons. The low momentum electrons are present in the defects like free volumes. When there are more imperfections where positrons may be localized, the parameter S will be important. When there are more annihilation events involving core electrons, the value of W increases. Momentum core electrons are mainly responsible for the energy area from 511 ± 5 keV and above.

Therefore, any changes in the S-parameter as a function of fluence will be associated with changes in free volume structure [52]. The values of S — as shown in Fig. 2 — vary relative to the fluence

TABLE I

Positron annihilation lifetime data for alpha irradiated CR39.

Fluence $[\alpha/\mathrm{cm}^2]$	τ_1 [ns]	I_1 [%]	τ_2 [ns]	I_2 [%]	τ_3 [ns]	I_3 [%]	r_h [Å]	V [Å^3]	F_V [%]	σ [ns]
0	0.150	17.42 ± 0.20	0.360	60.98 ± 0.11	1.802 ± 0.008	21.60 ± 0.13	2.668	78.79	3.06	–
2.6×10^8	0.148	17.85 ± 0.20	0.360	59.85 ± 0.20	1.796 ± 0.008	22.31 ± 0.16	2.665	79.11	3.17	0.51
5.27×10^8	0.125	17.61 ± 0.13	0.360	60.11 ± 0.10	1.809 ± 0.009	22.28 ± 0.11	2.668	78.79	3.15	0.10
7.91×10^8	0.125	13.12 ± 0.07	0.342	62.68 ± 0.07	1.723 ± 0.009	24.19 ± 0.06	2.550	63.31	3.01	0.20
1.3×10^9	0.125	12.56 ± 0.10	0.342	65.16 ± 0.10	1.775 ± 0.007	22.29 ± 0.10	2.668	78.79	3.16	0.20
1.84×10^9	0.125	13.32 ± 0.07	0.342	62.20 ± 0.07	1.784 ± 0.006	21.90 ± 0.11	2.650	77.78	3.06	0.20
3.6×10^9	0.150	17.26 ± 0.30	0.360	61.05 ± 0.30	1.802 ± 0.007	21.70 ± 0.15	2.631	76.04	2.97	0.41

of alpha irradiation, reaching a minimum value of 0.46781 at a fluence of 7.91×10^8. Conversely, the parameter W exhibits an inverse trend in the same range, reaching a maximum value of 0.0013 for the same fluence.

The increase in the parameter S signifies that the size of free volumes increases, which might be caused by an expansion through and between molecular chains as a result of the augmentation of the bond-scission cross-section. In contrast, the observed decrease may indicate a reduction either in the number or size of free volumes in the system. The reduction of these free volumes is significantly influenced by the cross-section of cross-linking. Since S characterizes the low-density regions, and W characterizes the high-density regions, the inverse relationship between them confirms the role of S in capturing changes in low-density regions while stressing the sensitivity of W to variations in high-density regions.

3.2. Positron annihilation lifetime spectra (PALS) analysis

PALS spectra are fitted with the LT 9.2 program [53]. The LT 9.2-based code essentially fits the experimental data to the following function

$$M(t) = \sum_i \frac{I_i}{\tau_i} \exp\left(-\frac{t}{\tau_i}\right), \tag{1}$$

and M is defined as a linear combination of exponential lifetime components.

From the experiment, we obtain a spectral data

$$y_{ex}(t) = \int_0^\infty \mathrm{d}t_0 \; R(t - t_0) M(t_0). \tag{2}$$

It is a convolution of the theoretical function (1) with the resolution function R.

We employed a single 270 ps Gaussian component as a resolution function when fitting the lifetime spectra. We have decided to use a two-component source correction. The first source component, τ_{1S}, equivalent to 380 ps, is related to Kapton foil annihilations. The second source component, τ_{NaCl} of 2.07 ns, was assumed to be the result of annihilations associated with the NaCl crystallites. The source contribution to the spectrum was 33.07%. The ratio of background to signal was 0.27%.

In reality, it has been established that the positron state that might exist in the network structure of the CR39 polymer can be p-Ps, free positron, or o-Ps, as shown in Fig. 3, where a lifetime spectrum of unirradiated CR39 is presented. The long-lived component τ_3 has truly generated an important interest in structural modifications. The size of the free volume holes is strongly linked with this component. Information regarding the concentration of the free volume is contained in the intensity of the long-lived component. An understanding of the distribution of the free volume in the material could be obtained by knowing the intensity of this component. Changes in that intensity may reflect changes in free volume concentration, which in turn may be related to structural changes such as chain scission or cross-linking [54].

Following the spectrum fitting, we get the values of τ_1, τ_2, and τ_3, which correspond to the lifetimes of p-Ps, free positrons, and o-Ps, with regard to their intensities, as given in Table I. The lifetime τ_3 has a large value as a result of the annihilation of the positron from the o-Ps state and the electron in a pick-off process [55, 56].

In fact, τ_3 is related to the size of the holes. This correlation was initially applied to the study of crystalline solids and has since been expanded to include amorphous materials like polymers. The inverse lifetime or annihilation rate of o-Ps in matter can be expressed as follows

$$\tau^{-1} = \lambda = 4\pi r_0^2 c \int \mathrm{d}r \, n_+(r) n_-(r) g(n_+, n_-), \tag{3}$$

where $g(n_+, n_-)$ is the electron–positron pair-correlation function calculated at the point in a homogeneous two-component plasma with the positron (or o-Ps) density n_+ and the electron density n_-. The free volume radius r_h could be calculated from the lifetime of o-Ps using the model of Tao [57] and Eldrup [58]. According to this theory, o-Ps is a single particle without an intrinsic property. It is located in a spherical well with

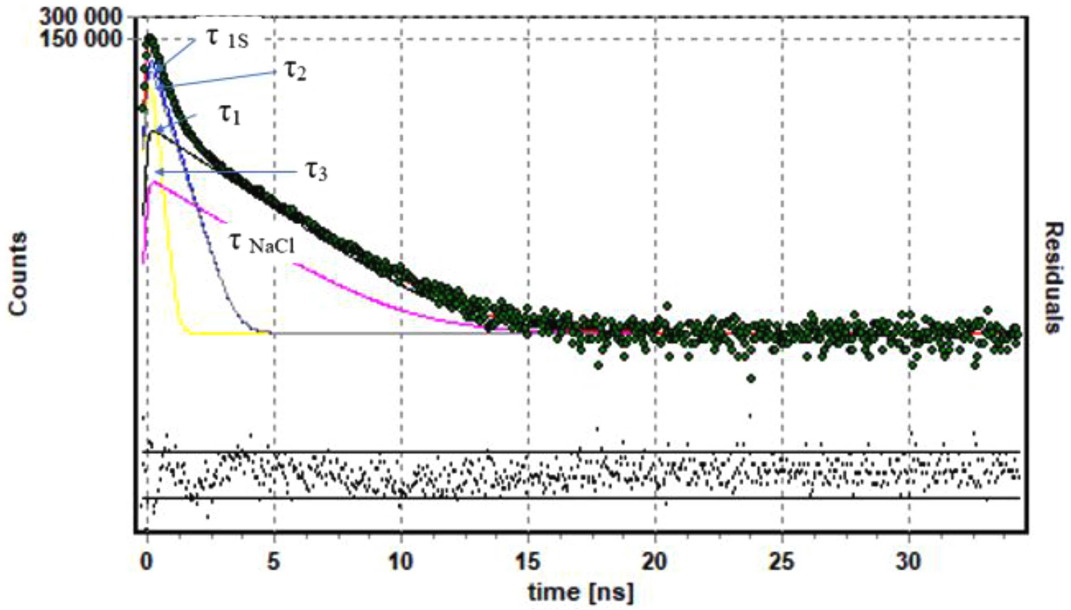

Fig. 3. Lifetime spectrum of unirradiated CR39.

an infinite potential barrier of radius r_0 and a homogenous electron layer δ_r between the hole radius r_h and r_0 (where $r_0 = r_h + \delta_r$). Then, $\tau_{(\text{o-Ps})}$ is related to r_h as follows

$$\lambda_{\text{o-Ps}} = 1/\tau_{(\text{o-Ps})} = \\ 2\,\text{ns}^{-1}\left[1 - \frac{r_h}{r_h+\delta_r} + \frac{1}{2\pi}\sin\left(\frac{2\pi r_h}{r_h+\delta_r}\right)\right]. \quad (4)$$

Here, $\delta_r = 0.166$ nm [59].

When fitting the recorded o-Ps lifetime values to (4) for geometrically known elliptic holes, a semiempirical equation is established [60]

$$\lambda_{\text{o-Ps}} = 1/\tau_{(\text{o-Ps})} = \\ 2\,\text{ns}^{(-1)}\left[1 - \frac{r_h}{r_h+\delta_r} + \frac{1}{2\pi}\sin\left(\frac{2\pi r_h}{r_h+\delta_r}\right) \otimes K\right], \quad (5)$$

where K is an additional function generalized for the modification of holes structure written like

$$K = \left(0.400s - 4.16s^2 + 2.76s^3\right)\left(l + 0.0018a\right). \quad (6)$$

Here, s is the eccentricity of the ellipsoid, i.e., $s = \sqrt{a^2 - b^2}/a$; a and b are the dimensions of the semimajor and minor axes, respectively. Furthermore, the formula (4) has been modified to account for various geometries, such as cuboids and cylinders [61, 62]. On the other hand, Schmitz and Müller-Plathe [63] suggested using pair potentials to calculate the total Ps potential in polymers, and then using the method of the path integral Monte Carlo approach to solve the resulting single-particle Schrödinger equation at limited temperature. Besides the single-particle approach, the existence of Ps state has been explored using accurate many-body *ab initio* techniques [64, 65]. In the context of the standard model of Tao and Eldrup, where the free volumes are almost spheres, the volumes of free volumes, V, of matching radius r_h are determined using the following equation $V = \frac{4\pi}{3}r_h^3$. Table I lists the values of r_h, V, and F_V, which represents the fraction of free volumes. The formula used to determine F_V is

$$F_V = C\,V_h I_3, \quad (7)$$

where $C = 0.0018$ [43].

According to the spectra analysis, the long-lived component τ_3 has a non-exponential character, which can be assigned to a lifetime distribution, carried on by a distribution of the size and shape of free volume holes. The continuous lifetime distribution analysis was made possible using LT 9.2 by incorporating a dispersion σ in the τ_3 value. The dispersions are mentioned in Table I for the irradiated samples. The standard deviation made a logarithmic Gaussian distribution of $\alpha_i(\lambda)$ of each i-th channel as follows [40]

$$\alpha_i(\lambda)\lambda\ \mathrm{d}\lambda = \frac{1}{\sigma_i\sqrt{2\pi}}\exp\left[-\frac{\left(\ln(\lambda)-\lambda_{i0}\ln(\lambda)\right)^2}{2\sigma_i^2}\right], \quad (8)$$

where

$$\lambda = 1/\tau_3. \quad (9)$$

Therefore, the free volume radius distribution, $f(R)$, could be modeled as demonstrated in Fig. 4 using the following formula [66]

$$f(R) = 2\Delta R\left[\cos\left(\frac{2\pi R}{R+\Delta R}\right) - 1\right]\frac{\alpha(\lambda)}{(R+\Delta R)^2}. \quad (10)$$

Figure 5 displays the τ_3 and r_h variations against alpha particle fluencies.

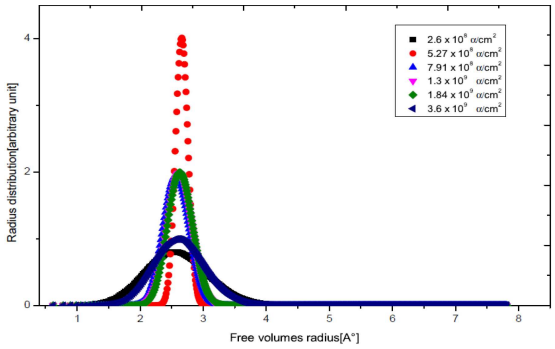

Fig. 4. Free volume radius distribution.

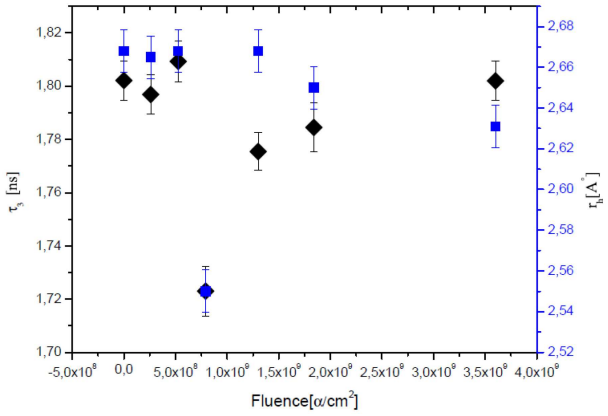

Fig. 5. Variation of τ_3 and free volume radius, r_h, vs fluence.

One notes a decrease between the unirradiated sample and the third fluence value, from $1.8025 \pm 9.4 \times 10^{-3}$ to $1.7231 \pm 9.4 \times 10^{-3}$ ns, followed by an increase to the fourth fluence value, where τ_3 assumes the value of $1.7772 \pm 9.4 \times 10^{-3}$ ns after which it stabilizes. The decrease or increase of the long-lived component is almost always correlated with the change in free volume radius and their concentration in the network structure [37]. The profile variation of the free volume radius has the same behavior as that of τ_3. There is a decrease between the unirradiated sample and the third fluence value, from 2.668 to 2.550 Å, and then there is an increase to the fourth fluence value, where the radius gets the value of 2.668 Å. Moreover, the intensity of the long-lived component increases from 21.6 to 24.19% in the same range of free volume radius decrease. The alpha particle effects could be expressed as a function of τ_3 or the free volume radius. When the probability of overlapping between induced radicals is predominant, the cross-linking yield will increase. Therefore, the long-lived component τ_3 can be decreased. In the case when the damaged regions are spatially separated as a result of the randomly distributed deposited energy, we note an increase in the free volume radius, which can be attributed to the higher probability of bond scission [5].

3.3. Theoretical calculation

From the SRIM simulation, we can see the depth of alpha particles inside CR39. This gives us a range of around 22 μm for $E_\alpha = 4.1$ MeV, where the Bragg curve peak found for it at 0.9 MeV provides the maximal value of electronic loss energy, as demonstrated in Fig. 6.

The radial distribution of alpha doses around their trajectory was obtained with Waligorski calculation [67, 68]. The the variation of the dose distribution according to such fluence was well displayed in Fig. 7.

This distribution is the result of approaching the doses deposited inside the cylinder around the particle's trajectory forming the track core. During the simulation, the value of the radii was changed from 1 to 10 nm for each fluence. We concluded that the dose distribution reaches its outermost radial limit, called the track core radii, at 5 nm.

The track core contains broken chemical bonds, which leads to the formation of free volumes. Moreover, it may include chain ends and new chemical entities resulting from cross-linking or bond scission. According to the performed simulation, the

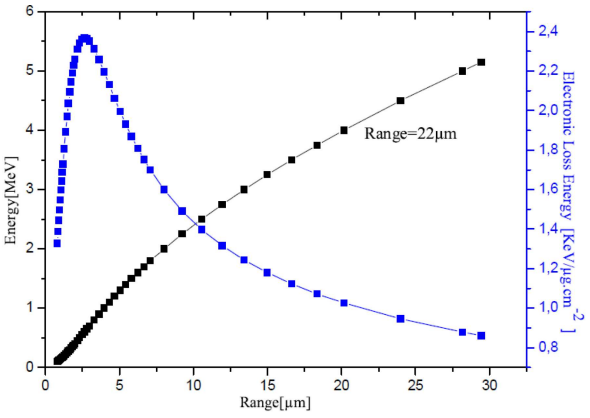

Fig. 6. Bragg curve and alpha energy vs range.

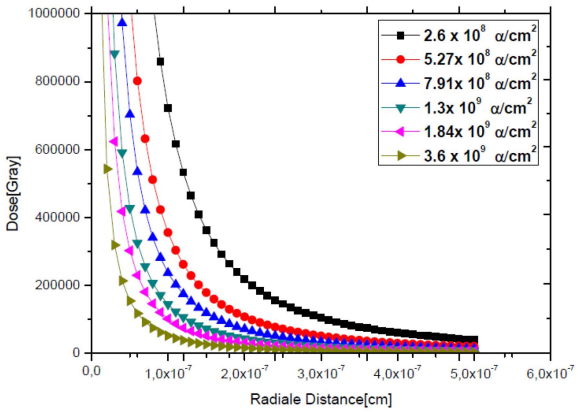

Fig. 7. Radial dose distribution vs radial distance.

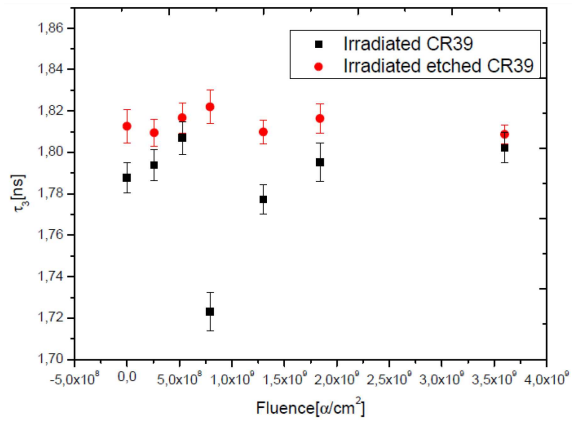

Fig. 8. Variation of τ_3 vs fluence for etched and no-etched samples.

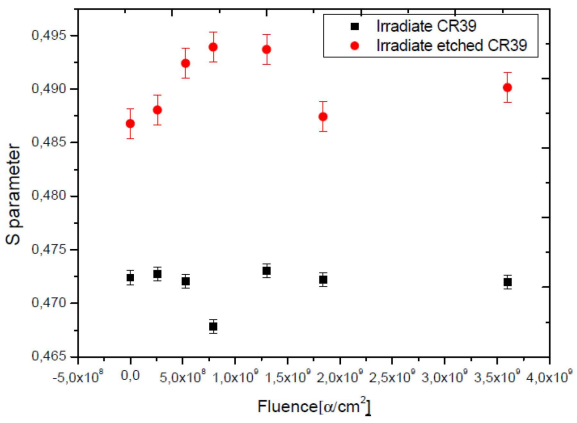

Fig. 10. Variation of S-parameter vs fluence for etched and no-etched samples.

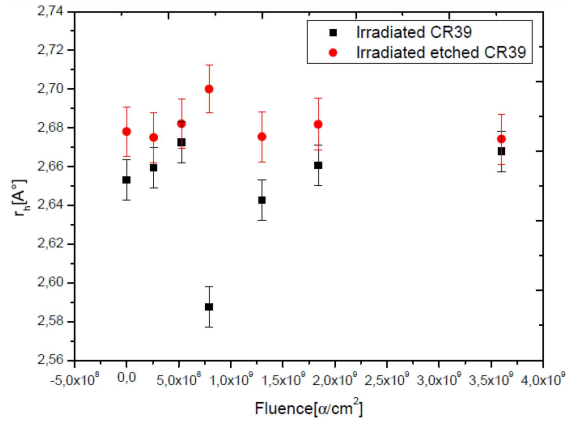

Fig. 9. Variation of free volume-radius vs fluence for etched and no-etched samples.

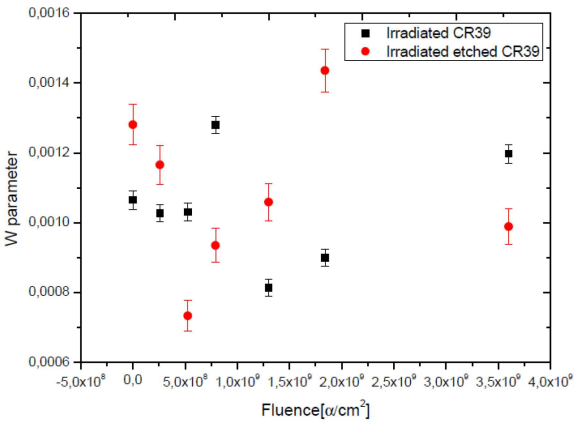

Fig. 11. Variation of W-parameter vs fluence for etched and no-etched samples.

TABLE II

Shown are the fraction of free volumes for irradiated samples — F_V; the total free volumes radius — rF_V; the new calculated free volumes fraction — $F_V{}'$.

Fluence [α/cm^2]	F_V (PAS) [%]	rF_V [Å]	$F_V{}' = \frac{V_{FV}}{V_{TC}}$ [%]
2.6×10^8	3.17	8.44	2.84
5.27×10^8	3.15	8.4	2.82
7.91×10^8	3.01	7.67	2.35
1.3×10^9	3.16	8.43	2.84
1.84×10^9	3.06	8.1	2.62
3.6×10^9	2.97	7.81	2.43

track core is distributed inside a cylinder with a radius of $r = 5$ nm, and its length corresponds to the range of alpha particles, $R_p = 22$ μm.

In order to assess how accurate this model is, we prepare the following calculation. In the context of the model, we assume that all the free volumes are contained within a cylinder of radius r and length l. The length of the cylinder is equal to the range of alpha particles, R_p. The radius is equivalent to the total free volume radius. The total free volume radius could be obtained by multiplying the free volume radius of each sample with its associated free volume fraction F_V. The volume of the cylinder containing all the free volumes, V_{FV}, is calculated as $V_{FV} = \pi(r_h F_V)^2 R_p$, and the track core volume is $V_{TC} = \pi(5)^2 R_p$. Dividing V_{FV} by V_{TC}, we obtain the quantity $F_V{}'$, which agrees by 78–89% with F_V. Table II presents the values of F_V, rF_V, and $F_V{}'$. Indeed, the obtained $F_V{}'$ values have a considerable level of concurrence with the free volume fractions obtained using PALS, indicating a reasonable agreement between the radial damages distribution and the PALS results.

3.4. Effects of etching on the S and W parameters and the positronium lifetime/free volume radius

Using the PAS technique, we can characterize the latent tracks via the parameter of free volume radius or the S-parameter, without an obligated need to reveal the latent tracks so that they can somehow be visualized under the microscope. Alternatively, we

prepare an experiment where the samples are etched for 5 min, and then PALS and DBS measurements are carried out. In Figs. 8, 9, 10, and 11, respectively, the profile variation of τ_3, the free volumes radius, the S-parameter, and the W-parameter have been shown for both the etched and no etched samples.

In Fig. 10, a significant increase is marked for the etched samples. In turn, a slight increase is noted in Figs. 8 and 9. Regarding the variation of the W-parameter for the etched samples, we note an inverse dependency on fluences compared to no-etched samples.

We relate the difference between S-parameter and the long-lived component of τ_3 to the fact that S is more sensitive to electron density variation than τ_3. There is clearly a difference in the change in the annihilation parameters of the etched samples, which demonstrates the sensitivity of PAS in monitoring birth tracks. The latter result could not ever be seen with an optical microscope (OM), where an hour of etching is the minimum time to get the tracks visualized under OM [22], or even 2 hours, as done in [69]. We think that the sensitivity of PAS towards detecting birth tracks might be used to do an extrapolation between the free volume radius and the track diameter if we take a small step of etching treatment for a longer time range.

4. Conclusions

The presented study set out to investigate the effect of alpha particles on CR39 by examining changes in free volumes within the network structure. PALS and DBS techniques have been employed to achieve this. PALS is an effective tool for studying free volumes in materials by measuring the spatial features. DBS is an additional method that offers insightful information on the momentum density distribution. We conducted theoretical calculations of the radial dose distribution to verify the experimental results acquired using PALS. This enabled us to validate the PALS measurements. The study also went a step further by doing the analysis again after five minutes of etching the CR39 polymer. Important details regarding the structural modifications in birth tracks following the etching process were gained by this etching study. The findings were interesting and offered important information on how CR39 behaved when exposed to alpha particles. First, it was found that the behavior of the free volume radius closely matched the S-parameter obtained from DBS. This resemblance revealed a strong complementarity between the two approaches, which aided in the development of a more thorough knowledge of the response of the system to alpha particles. The fraction of free volume concentration can be estimated using the Waligorski model. There is an excellent agreement between theoretical calculations and PALS data. This agreement demonstrated the accuracy and dependability of the PALS method for analyzing track parameters and served as an important experimental methodology validation. Another important outcome was the demonstration of the capacity of PALS to precisely record changes in the angstrom size of latent tracks produced by alpha irradiation. The sensitivity and potential of PALS as a unique tool for evaluating radiation damage is highlighted by its capacity to detect and evaluate such modification types. The study further expanded on its analysis to examine changes in angstrom size for birth tracks after the etching procedure. The findings demonstrated that PALS is also useful in capturing these changes, thus emphasizing its applicability as a dependable method for describing the development of the birth track.

Finally, the spectrum of free volume radius was proven to be a useful predicting tool for alpha particle fluencies using CR39 under identical irradiation conditions. A deeper comprehension of the response of the CR39 to alpha particle irradiation was achieved. This understanding opened up potential applications for researching the effects of ionizing radiation and made significant contributions to the field of alpha particle dosimetry.

References

[1] B.G. Cartwright, E.K. Shirk, P.B. Price, *Nucl. Instrum. Methods* **153**, 457 (1978).

[2] A.F. Saad, E.M. Sedqy, R.M. Ahmed, *Nucl. Instrum. Methods Phys. Res. B* **485**, 41 (2020).

[3] M. Fromm, S. Kodaira, T. Kusumoto, R. Barillon, T. Yamauchi, *Polym. Degrad. Stab.* **161**, 213 (2019).

[4] A.F. Saad, M. Fromm, M.H. Ibraheim, A.A. El-Namrouty, A.M. Nwara, S.A. Kandil, M.S. Dawood, *Radiat. Phys. Chem.* **187**, 109579 (2021).

[5] R. Kumar, S. Rajguru, D. Das, R. Prasad, *Radiat. Meas.* **36**, 151 (2003).

[6] J.F. Ziegler, J.P. Biersack, M.D. Ziegler, SRIM, 2003.

[7] L. Torrisi, L. Silipigni, M. Cutroneo, E. Proverbio, A. Torrisi, *Vacuum* **203**, 111240 (2022).

[8] R. Katz, E.J. Kobetich, *Radiat. Eff.* **3**, 169 (1970).

[9] R. Katz in: *9th Int. Conf. on Solid State Nuclear Track Detectors and Meeting of the Working Group on Space Biophysics of the Council of Europe*, 1976.

[10] El-Sayed Awad, A. Salah, M. Abu-Shady, S. Hassan, *Radiat. Phys. Chem.* **206**, 110771 (2023).

[11] R. Katz, E.J. Kobetich, *Phys. Rev.* **186**, 344 (1969).

[12] H. Dertinger H. Jung, *Molecular Radiation Biology: The Action of Ionizing Radiation on Elementary Biological Objects*, Springer, 2013.

[13] Z. Lounis-Mokrani, A. Badreddine, D. Mebhah, D. Imatoukene, M. Fromm, M. Allab, *Radiat. Meas.* **43**, S41 (2008).

[14] S.-L. Guo, B.-L. Chen, S.A. Durrani, in: *Handbook of Radioactivity Analysis*, Elsevier, 2020, p. 307.

[15] J. Wang, Y. Zhou, L. Jiang, *ACS Nano* **15**, 18974 (2021).

[16] E. Dartyge, J.P. Duraud, Y. Langevin, M. Maurette, *Phys. Rev. B* **23**, 5213 (1981).

[17] X.-F. Jiang, J.-R. Zhou, H. Luo et al., *Nucl. Sci. Tech.* **33**, 89 (2022).

[18] T. Yamauchi, N. Yasuda, T. Asuka, K. Izumi, T. Masutani, K. Oda, R. Barillon, *Nucl. Instrum. Methods Phys. Res. B* **236**, 318 (2005).

[19] T. Yamauchi, R. Barillon, E. Balanzat, T. Asuka, K. Izumi, T. Masutani, K. Oda, *Radiat. Meas.* **40**, 224 (2005).

[20] T. Yamauchi, S. Watanabe, A. Seto, K. Oda, N. Yasuda, R. Barillon, *Radiat. Meas.* **43**, S106 (2008).

[21] D. Hermsdorf M. Hunger, *Radiat. Meas.* **44**, 766 (2009).

[22] Z. Lounis, S. Djeffal, K. Morsli, M. Allab, *Nucl. Instrum. Methods Phys. Res. B* **179**, 543 (2001).

[23] N.F. Kadhim, A.A. Ridha, M.D. Salim, M.Y. Hanfi, Y.A. Mostafa, *Mater. Today Proc.* **44**, 2903 (2021).

[24] A.M. Abdalla, T.I. Al-Naggar, R.H. Alhandhal, H.B. Albargi, *Nucl. Instrum. Methods Phys. Res. A* **1042**, 167419 (2022).

[25] V.P. Shantarovich, *J. Membrane Sci. Res.* **8**, 1 (2022).

[26] J. Kong, J. Liu, P. Jia, N. Qi, Z. Chen, S. Xu, N. Li, *J. Membrane Sci.* **645**, 120163 (2022).

[27] G. Dlubek, D. Kilburn, V. Bondarenko, J. Pionteck, R. Krause-Rehberg, M.A. Alam in: *24th Arbeitskreistagung "Nichtkristalline Structuren" of DGK*, 2003, p. 203.

[28] S. Cheng, Z. Wojnarowska, M. Musiał, S. Kołodziej, E. Drockenmuller, M. Paluch, *Polymer* **212**, 123286 (2021).

[29] P. Utpalla, S.K. Sharma, K. Sudarshan, M. Sahu, P.K. Pujari, *Solid State Ionics* **339**, 114990 (2019).

[30] F.A. Selim, *Mater. Charact.* **174**, 110952 (2021).

[31] M.J. Puska, R.M. Nieminen, *Rev. Mod. Phys.* **66**, 841 (1994).

[32] G. Dlubek, D. Kilburn, V. Bondarenko, J. Pionteck, R. Krause-Rehberg, M.A. Alam, *Macromol. Symp.* **210**, 11 (2004).

[33] A. Tanwar, "Micro-Structural Properties of Polymers by PALS — A Review", (2017).

[34] M. Charlton J.W. Humberston, *Positron Physics*, Cambridge University Press, 2000.

[35] O.E. Mogensen, *Positron Annihilation in Chemistry*, Springer, 2012.

[36] J. Nico, D. Gidley, A. Rich, P. Zitzewitz, *Phys. Rev. Lett.* **65**, 1344 (1990).

[37] A. Dupasquier A.P. Mills Jr., *Positron Spectroscopy of Solids*, Vol. 125, IOS press, 1995.

[38] G. Dlubek, J. Stejny, T. Lüpke, D. Bamford, K. Petters, C. Hübner, M.A. Alam, M.J. Hill, *J. Polym. Sci. B Polym. Phys.* **40**, 65 (2001).

[39] V. Krsjak, T. Shen, J. Degmova, S. Sojak, E. Korpas, P. Noga, W. Egger, B. Li, V. Slugen, F.A. Garner, *J. Mater. Sci. Technol.* **105**, 172 (2022).

[40] Z. Lounis-Mokrani, A. Guittoum, D. Imatoukene, M. Aitziane, A. Badreddine, M. Mebhah, *Radiat. Meas.* **50**, 26 (2013).

[41] R. Kumar, S.A. Ali, A.K. Mahur, D. Das, A.H. Naqvi, H.S. Virk, R. Prasad, *Nucl. Instrum. Methods Phys. Res. B* **244**, 257 (2006).

[42] R. Kumar, U. De, P.M.G. Nambissan, M. Maitra, S.A. Ali, T.R. Middya, S. Tarafdar, F. Singh, D.K. Avasthi, R. Prasad, *Nucl. Instrum. Methods Phys. Res. B* **266**, 1783 (2008).

[43] R. Kumar, P. Singh, S.K. Gupta, R. Gupta, M.K. Jaiswal, M. Prasad, A. Roychowdhury, R.P. Chauhan, D. Das, *J. Radioanal. Nucl. Chem.* **314**, 1659 (2017).

[44] S. Mesbah, K. Abib, A. Guittoum, M. Akou, I. Bibimoune, D. Bradai, *MRS Commun.* **13**, 350 (2023).

[45] H. Elazhar, A.C. Chami, M. Abdesselam, N. Arbor, D. Muller, A. Nasreddine, M. Roumie, Z. El Bitar, A. Nourreddine, *Nucl. Instrum. Methods Physics Res. B* **448**, 52 (2019).

[46] M.A. Al-Jubbori, M. Fromm, E.M. Awad, *Nucl. Instrum. Methods Phys. Res. A* **1005**, 165402 (2021).

[47] A.A. Azooz, M.A. Al-Jubbori, *Nucl. Instrum. Methods Phys. Res. B* **316**, 171 (2013).

[48] I.K. MacKenzie, J.A. Eady, R.R. Gingerich, *Phys. Lett. A* **33**, 279 (1970).

[49] P.E. Mallon, D.M. Schrader, Y.C. Jean, *Principles and Applications of Positron and Positronium Chemistry*, World Scientific Publishing, Singapore 2003.

[50] J. Dryzek, Sp-1 program, 2004.

[51] J. Dryzek M. Wróbel, *Wear* **466–467**, 203524 (2021).

[52] O. Moutanabbir, R. Scholz, U. Gösele, A. Guittoum, M. Jungmann, M. Butterling, R. Krause-Rehberg, W. Anwand, W. Egger, P. Sperr, *Phys. Rev. B* **81**, 115205 (2010).

[53] J. Kansy D. Giebel, *J. Phys. Conf. Ser.* **265**, 012030 (2011).

[54] L. Chiari, M. Nippa, Y. Ikeda, T. Sato, Y. Tsujimoto, A. Kato, N. Chiba, M. Fujinami, *J. Appl. Polym. Sci.* **139**, e52857 (2022).

[55] C.A. Furtado, G.G. Silva, J.C. Machado, M.A. Pimenta, R.A. Silva, *J. Phys. Chem. B* **103**, 7102 (1999).

[56] I. Irska, S. Paszkiewicz, D. Pawlikowska, J. Dryzek, A. Linares, A. Nogales, T.A. Ezquerra, E. Piesowicz, *Polymer* **229**, 123949 (2021).

[57] S.J. Tao, *J. Chem. Phys.* **56**, 5499 (1972).

[58] M. Eldrup, D. Lightbody, J.N. Sherwood, *Chem. Phys.* **63**, 51 (1981).

[59] J. Bohlen, J. Wolff, R. Kirchheim, *Macromolecules* **32**, 3766 (1999).

[60] Y.C. Jean, J.D. Van Horn, W.-S. Hung, K.-R. Lee, *Macromolecules* **46**, 7133 (2013).

[61] B. Jasinska, A.E. Kozioł, T. Goworek, *J. Radioanal. Nucl. Chem.* **210**, 617 (1996).

[62] A. Zubiaga, M.M. Ervasti, I. Makkonen, A. Harju, F. Tuomisto, M.J. Puska, *J. Phys. B At. Mol. Opt. Phys.* **49**, 064005 (2016).

[63] H. Schmitz, F. Müller-Plathe, *J. Chem. Phys.* **112**, 1040 (2000).

[64] A.R. Swann, G.F. Gribakin, *Phys. Rev. A* **101**, 022702 (2020).

[65] J. Hofierka, B. Cunningham, C.M. Rawlins, C.H. Patterson, D.G. Green, *Nature* **606**, 688 (2022).

[66] A. Nyczyk-Malinowska, E. Dryzek, M. Hasik, J. Dryzek, *J. Mol. Struct.* **1065–1066**, 254 (2014).

[67] M.P.R. Waligórski, R.N. Hamm, R. Katz, *Int. J. Radiat. Appl. Instrum. D* **11**, 309 (1986).

[68] J.L. Wormald, A.I. Hawari, *J. Nucl. Mater.* **566**, 153797 (2022).

[69] G. Gillmore, D. Wertheim, S. Crust, *Sci. Total Environ.* **575**, 905 (2017).